Appl Phys A (2014) 114:1189–1193
DOI 10.1007/s00339-013-7819-8

Applied Physics A
Materials Science & Processing

Controlled growth of standing Ag nanorod arrays on bare Si substrate using glancing angle deposition for self-cleaning applications

Dhruv P. Singh · J.P. Singh

Received: 8 March 2013 / Accepted: 13 June 2013 / Published online: 2 July 2013

Abstract A facile approach to manipulate the hydrophobicity of surface by controlled growth of standing Ag nanorod arrays is presented. Instead of following the complicated conventional method of the template-assisted growth, the morphology or particularly average diameter and number density (nanorods cm^{-2}) of nanorods were controlled on bare Si substrate by simply varying the deposition rate during glancing angle deposition. The contact angle measurements showed that the evolution of Ag nanorods reduces the surface energy and makes an increment in the apparent water contact angle compared to the plain Ag thin film. The contact angle was found to increase for the Ag nanorod samples grown at lower deposition rates. Interestingly, the morphology of the nanorod arrays grown at very low deposition rate (1.2 Å sec^{-1}) results in a self-cleaning superhydrophobic surface of contact angle about 157° and a small roll-off angle about 5°. The observed improvement in hydrophobicity with change in the morphology of nanorod arrays is explained as the effect of reduction in solid fraction within the framework of Cassie–Baxter model. These self-cleaning Ag nanorod arrays could have a significant impact in wide range of applications such as anti-icing coatings, sensors and solar panels.

1 Introduction

The surface which exhibits an apparent water contact angle $>150°$ and a roll-off angle $<10°$ is normally considered as self-cleaning superhydrophobic surface [1–4]. The self cleaning property of these superhydrophobic surfaces makes them ideal for various practical applications such as impermeable textiles, anti-icing coatings, biomedical drug delivery, and solar panels [5–9]. It is now well established that such superhydrophobic surfaces can be made by employing two kinds of approaches: creating a porous or the solid–air composite surface by synthesis of micro- and nanostructures of a hydrophobic material or by chemically modifying the porous surface with a low surface energy material [1, 8–14]. Recently, glancing angle deposition (GLAD) has emerged as a simple and versatile technique to modify the surface with the growth of standing nanorod arrays [15–23]. The nanorods constitute a porous surface and researchers have observed that they can be used to fabricate the hydrophobic surface of various materials [24–28]. In an interesting research, Fan and Zhao [26] have observed that the coating of Si nanorod arrays with a hydrophobic material followed by piranha treatment forms the bunches of nanorods on the surface, which gives a high contact angle about 167° and roll-off angle about 2°. Khedir et al. [27] have shown that the coating of Tf on W nanorods can make the surface superhydrophobic. They observed that by controlling the substrate tilt angle or pressure during GLAD, the apparent water contact angle of nanorods film can be tuned. Although these works show the possibility to use GLAD for making a superhydrophobic surface, their processes involve some kind of coating or chemical surface treatment of the nanorod films. The use of such multistep surface treatments makes the surface modification process complex and time consuming.

In this study, we report a simple and single-step approach to manipulate the hydrophobicity of surface by controlling the morphology of standing Ag nanorod arrays. The morphology of nanorod arrays on bare Si substrate was controlled by varying the deposition rate during GLAD. Nature of water interaction with the Ag nanorod arrays was inves-

D.P. Singh · J.P. Singh (✉)
Department of Physics, Indian Institute of Technology Delhi, Hauz Khas, New Delhi 110016, India
e-mail: jpsingh@physics.iitd.ac.in

tigated by measuring the static contact angle. It was found that the evolution of Ag nanorods reduces the surface energies and makes an increment in the apparent water contact angle compared to the plain Ag thin film. We have shown that, by controlling the morphology of Ag nanorod arrays, the surface energy can be reduced sufficiently to produce a superhydrophobic surface with the self-cleaning properties.

2 Experimental details

The nanorod arrays were grown over Si (100) substrates by thermal evaporation of Ag powder (99.95 %) using GLAD method. For the growth of Ag nanorods, the substrates were inclined in the polar direction such that the substrate normal made a very high angle ($\alpha = 85°$) with the direction of incident vapor flux. During deposition, the pressure in the GLAD chamber was better than 2×10^{-6} Torr, and the substrates were kept at room temperature (∼30 °C). The deposition rate was adjusted by varying input power to the thermal deposition boat. The film thickness and deposition rate was monitored by a quartz crystal microbalance (QCM) positioned at normal incidence to the vapor source. In order to observe the effect of deposition rate on morphology of Ag nanorod arrays, the other growth parameters such as substrate temperature and source to substrate separation were kept same for all the samples. Analysis of film morphology was done using scanning electron microscope (SEM, ZEISS EVO 50). To study the effect of nanorod morphology on surface wetting behavior, the droplets of deionized (DI) water of 3 µL volume were deposited on the samples. The image of droplet on sample was captured using a CMOS camera equipped with a magnifying lens. The contact angle of droplet on Ag samples was measured using the *Image J* software (National Institute of Health, USA). The contact angle measurements were repeated five times at different positions of each sample.

3 Results and discussion

3.1 Controlled growth of Ag nanorod arrays on bare Si substrate

The deposition rate was examined as a potential growth parameter to control the morphology of Ag nanorod arrays on bare Si substrate during GLAD. For this study, the growth was done at different deposition rates varying from 14.6 Å sec^{-1} to 1.2 Å sec^{-1}. The SEM micrographs of Ag samples grown at different deposition rates are shown in Fig. 1. It can be observed from the SEM images that the deposition rate significantly affects the morphology or particularly the size and lateral distribution of the Ag nanorods

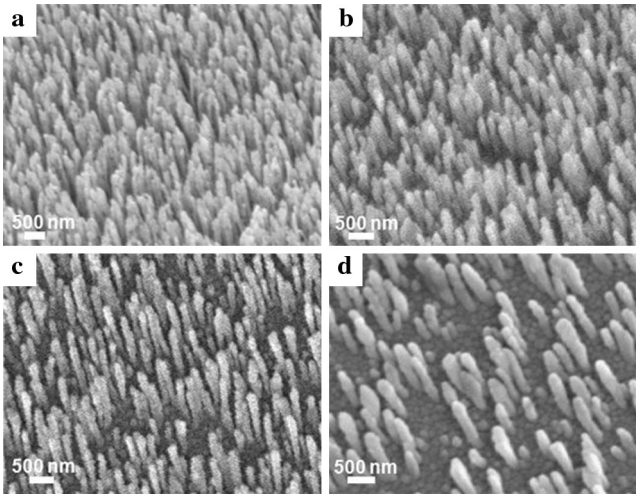

Fig. 1 SEM images of Ag nanorod films grown at different deposition rates (Å sec^{-1}): (**a**) 14.6, (**b**) 8.2, (**c**) 4.1, and (**d**) 1.2

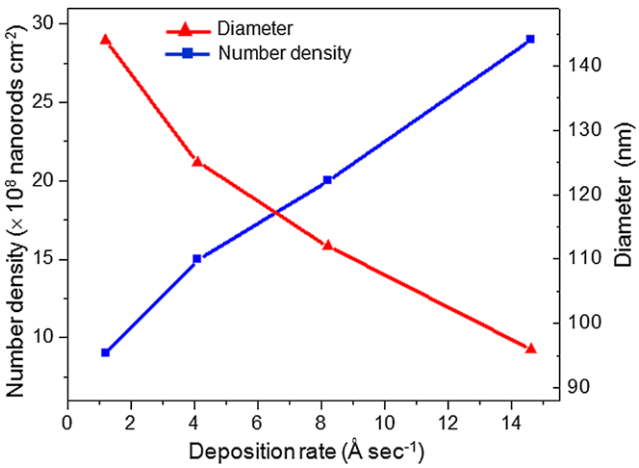

Fig. 2 Deposition rate dependence of the number density and average diameter of the nanorods

on bare substrate. The variation in size and distribution was calculated in terms of the average diameter and number density (nanorods cm^{-2}) of the nanorods. Figure 2 plots these parameters as functions of the deposition rate. It shows that the density of nanorods decreases to about one-third from 29×10^8 nanorods cm^{-2} to 9×10^8 nanorods cm^{-2}, while the diameter of nanorods increases from 96 ± 16 nm to 144 ± 25 nm, when deposition rate varies from 14.6 Å sec^{-1} to 1.2 Å sec^{-1}.

During GLAD, the initial stage atomic nucleation and then evolution of the surface consisting of three-dimensional particles or islands are very crucial [15, 16, 21]. Since, these atomic nuclei or islands act as the nucleation centers and with continuous supply of atomic flux, they evolve in the form of nanorods following the direction of the incoming flux. Therefore, if somehow the size and distribution of the nucleation centers get affected in the initial growth stage,

then the similar change may appear in the morphology of the finally grown nanorods film [21, 29–31]. The size and density of these nucleation centers is basically decided by the surface diffusion of adatoms [21, 31, 32]. If the adatom surface diffusion is high, then the lateral size of nucleation centers increases [31, 32]. In this case, the closely spaced small islands or nuclei get coalesced to form the bigger islands, and consequently, this process also reduces the number density of islands on the surface. The surface diffusion strongly depends on the surface temperature and the energy of adatom. But, in addition to these more significant parameters, it has been observed that the deposition rate can also control the adatom surface diffusion [31–33]. It can be understood in terms of the probability of adatoms to move over the surface without getting buried underneath the forthcoming adatoms, which is decided by the value of deposition rate. It has been shown that the average adatom diffusion distance varies inversely with the deposition rate [30]. This means that the decrease in deposition rate simply results in the increase of adatom surface diffusion, which in turn will induce the formation of a surface consisting of the nucleation centers of larger size but smaller number density during the initial stage growth. This deposition-rate-dependent change in the morphology of nucleation centers in the initial growth stage simply leads to the evolution of nanorods with increased diameter and reduced surface density on lowering the deposition rate as observed in the present study [21, 31]. Here it is necessary to discuss that in GLAD, the columnar growth can be possible only if the adatoms reaching to surface at an inclined path follow the shadowing effect [15, 21, 30, 31]. To maintain this shadowing effect, adatoms should have a limited surface diffusion [21, 30, 31]. Therefore, if we decrease the deposition rate to a very low value, then the resulting large surface diffusion may diminish this necessary shadowing effect, and in that case we may not be able to get the desired columnar growth.

3.2 Contact angle measurements and modeling

The effect of diameter and lateral distribution of Ag nanorods on the surface wetting behavior was investigated by performing the contact angle measurements with a sessile water droplet. The contact angle measurements of Ag nanorod samples grown at different deposition rates are shown in Fig. 3. The apparent water contact angle on plain Ag thin film was found to be 92.5°, while in the case of Ag nanorod samples the minimum contact angle recorded was about 104°. This indicates that the evolution of nanorods makes the surface hydrophobic. In addition, the change in morphology of nanorods also appears to affect the contact angle, and it can be observed that the contact angle increases for the Ag nanorod samples grown at lower deposition rates. Interestingly, at the very low deposition rate (1.2 Å $\sec^{-1}$)

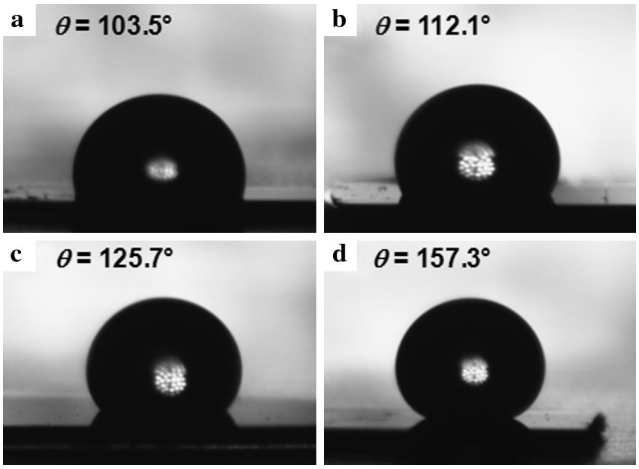

Fig. 3 Contact angle measurements of nanorod arrays grown at different deposition rates (Å $\sec^{-1}$): (**a**) 14.6, (**b**) 8.2, (**c**) 4.1, and (**d**) 1.2

the contact angle increases to about 157°. This value of contact angle indicates the formation of a superhydrophobic surface. Figure 4a shows the anti-adhesion behavior of this superhydrophobic surface. The approach, contact, and departure processes of a 3 μL water droplet suspending on a syringe with respect to the surface were carried out, and the direction of movement is shown by red arrows. It can be seen that water droplet may easily and completely depart from the surface without wetting or leaving any residue on the surface, indicating good anti-adhesion ability. Also, when we deposit the droplet on the inclined surface, it completely rolls off (Fig. 4b). The roll-off angle of this surface was found to be about 5°. These observations simply indicate that the nanorods film grown at smaller value of deposition rate (1.2 Å $\sec^{-1}$) has the self-cleaning effect. It is important to discuss that, on further decreasing the deposition rate that is below 1.2 Å $\sec^{-1}$ the distorted columnar and coalesced island-type film morphology was observed. In that case, instead of sitting on the solid–air composite surface, the water droplet wets the complete solid surface, which results in the decrease of contact angle values.

The observed morphology-dependent change in contact angle on nanorod arrays can be explained using the Cassie–Baxter model [1, 34–36]. The model proposed that on nanostructured surface the water droplet can be considered to be sitting on a composite surface made up of solid and air. The presence of air in place of a solid surface simply reduces the effective surface energies responsible for the spreading of water on the surface, and hence it improves the hydrophobicity of surface. In this case, if the intrinsic contact angle of solid surface is θ_i, then the observed contact angle θ on nanostructured or solid–air composite surface can be calculated as

$$\cos\theta = f(1 + \cos\theta_i) - 1, \quad (1)$$

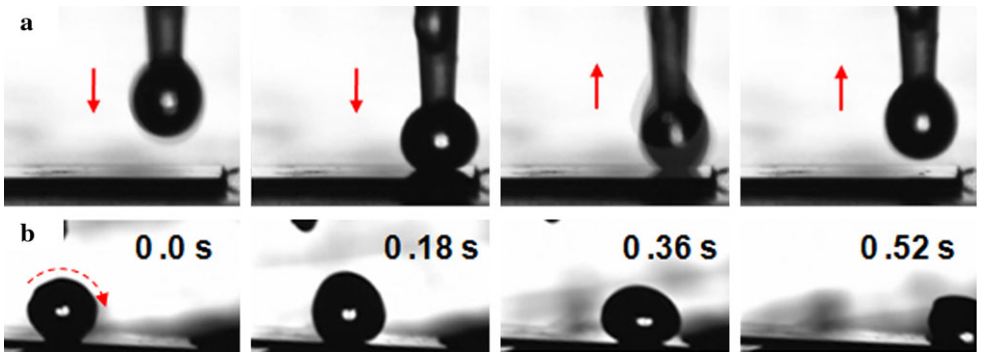

Fig. 4 (**a**) Anti-adhesion test: the water droplet suspended on a syringe is shown to touch the surface without wetting it. The *red arrows* represent the syringe's moving direction. (**b**) Roll-off test: the water droplet rolls of on the surface inclined at 5°. The time sequence of droplet on the surface is also marked

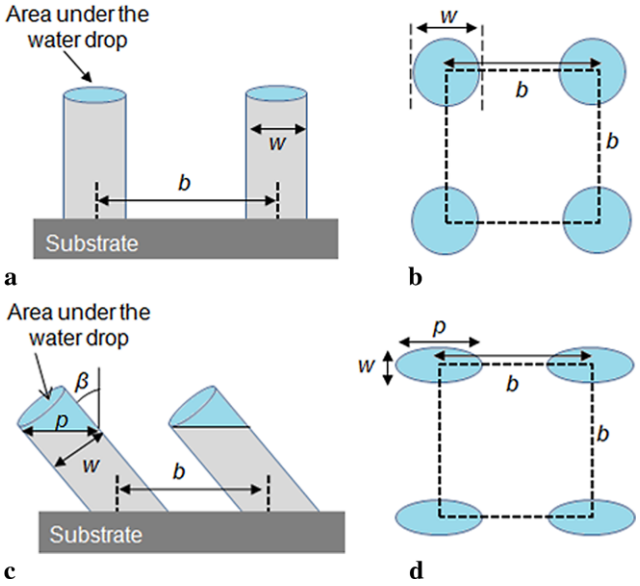

Fig. 5 (**a**) Schematic shows the wet area of vertically standing, cylindrical shape nanorods of diameter w, and inter-rod separation b. (**b**) Top view of these nanorods shows that if the rods are uniformly distributed, then only the circular top area $\pi w^2/4$ of one nanorod will contribute as liquid–solid interface area to the total liquid interface of base area b^2. (**c**) Wet area of nanorods inclined on the surface with angle β. (**d**) Top view of inclined nanorods showing the elliptical cross-section of wet area with minor axis as the diameter of nanorod w and major axes as p, which is equal to $w/\cos\beta$

where f is the solid fraction, defined as the area fraction of the liquid–solid interface [1, 34–36]. The relation clearly shows that any reduction in solid fraction f will result in the increment of observed contact angle θ. Now, if we consider a case of vertically standing and cylindrical shape nanorods of diameter w and inter-rod separation b and assume that the rods are uniformly distributed and the water droplet wets only the top of these nanorods, then the solid fraction of nanorods surface will be [37]

$$f = \frac{\pi w^2/4}{b^2}. \tag{2}$$

The schematic of above approximation and effective area in contact to the water droplet is shown in Figs. 5a and 5b. This relation was for vertically standing nanorods, but in our case the nanorods grow inclined. So, in that case the wet area of nanorods will be different. Considering a simple case, it was assumed that the droplet wets only the top surface of nanorods as marked in the schematic shown in Fig. 5c. This wet area forms an elliptical cross-section with minor axis as diameter of nanorod w and major axis as $w/\cos\beta$. In a simple approach this elliptical area can be considered as the liquid–solid interface area. The top view of these uniformly distributed inclined nanorods is shown in Fig. 5d. The surface area of one complete ellipse ($\pi w^2/4\cos\beta$) that is considered as the wet area of one nanorod will contribute as the liquid–solid interface to the total liquid interface of base area b^2. In that case, Eq. (2) will be modified as

$$f = \frac{\pi w^2}{4b^2\cos\beta}, \tag{3}$$

where β is the nanorod inclination angle with the substrate normal. The β can be calculated using the semi-empirical relation, $\beta = \alpha - \sin^{-1}((1-\cos\alpha)/2)$, where, α is the vapor incidence angle (85°) [38]. Using the values of average diameter w, average inter-rod separation b obtained from the SEM analysis, and the calculated value of β (58°) in Eq. (3), the solid fraction was calculated for the nanorod samples grown at different deposition rates. It was observed that the change in morphology of nanorods on lowering the deposition rate results in the decrement of solid fraction. The pattern of solid fraction with change in the deposition rate is shown in Fig. 6. If we consider the intrinsic contact angle θ_i as of the conventional Ag thin film (92.5°), then putting the value of solid fraction in Eq. (1), the observed contact angle θ can be calculated for all the nanorod samples. The calculated and experimentally measured values of contact angle of samples grown at different deposition rates are shown in Fig. 6. The framework of Cassie–Baxter model developed in this study considers few assumptions: (i) the nanorods are uniformly distributed, (ii) the nanorods have the same length and diameter, (iii) all the nanorods have same inclination angle β with respect to the substrate normal, and (iv) the water droplet wets only the top surface of the nanorods. Actually, the morphology of nanorods may deviate from these assumed conditions. This is the reason behind the deviation

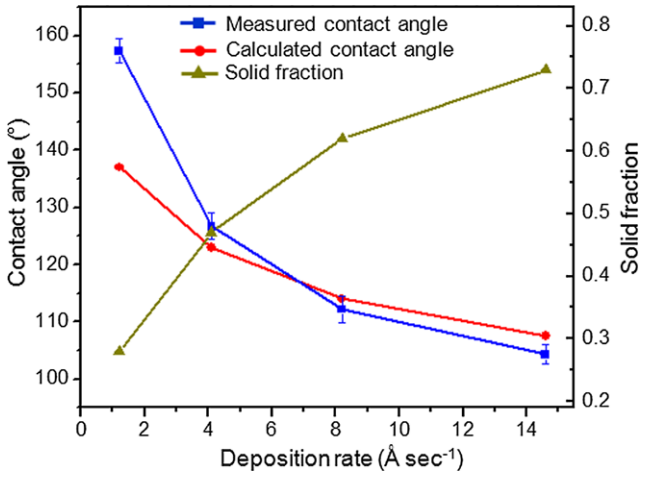

Fig. 6 Contact angles and calculated solid fraction as functions of the deposition rate of nanorod arrays

observed between the measured and calculated values of the contact angle. But, even then a similarity in the pattern of the calculated and experimentally measured contact angle values can be seen. It simply suggests that the observed enhancement in contact angle or hydrophobicity of nanorods film can be attributed to the effect of decrement in the solid fraction on lowering the deposition rate.

4 Conclusions

We have successfully demonstrated the approach of deposition rate to control the size and distribution of the Ag nanorods on a bare Si substrate during GLAD. The observed growth mechanism is considered as the effect of increase in adatom surface diffusion on lowering the deposition rate. Water wettability test showed that the evolution of Ag nanorods makes the surface hydrophobic and the hydrophobicity increases for the nanorod films grown at low deposition rate. At the lower deposition rate (1.2 Å $\sec^{-1}$) morphology of nanorods film forms a self-cleaning superhydrophobic surface with contact angle 157° and a small roll-off angle 5°. The observed improvement in hydrophobicity on nanorods film is explained as the effect of reduction in solid fraction within the framework of Cassie–Baxter model.

Acknowledgement D.P.S. kindly acknowledges CSIR, India for the research fellowship. This research was supported by the financial grant No. SR/S2/CMP-13/2010 DST and RP02395 from DIT, India.

References

1. D. Quere, Rep. Prog. Phys. **68**, 2495 (2005)
2. T. Sun, L. Feng, X. Gao, L. Jiang, Acc. Chem. Res. **38**, 644 (2005)
3. M. Ma, R.M. Hill, Curr. Opin. Colloid Interface Sci. **11**, 193 (2006)
4. Z. Guo, W. Liu, B.L. Su, J. Colloid Interface Sci. **353**, 335 (2011)
5. A. Nakajima, K. Hashimoto, T. Watanabe, Monatsh. Chem. **132**, 31 (2001)
6. B. Zhao, J.S. Moore, D.J. Beebe, Science **291**, 1023 (2001)
7. R. Blossey, Nature **2**, 301 (2003)
8. B. Bhushan, Y.C. Jung, K. Koch, Philos. Trans. R. Soc. A **367**, 1631 (2009)
9. K. Liu, L. Jiang, Annu. Rev. Mater. Res. **42**, 231 (2012)
10. H.Y. Erbil, A.L. Demirel, Y. Avci, O. Mert, Science **299**, 1377 (2003)
11. C. Guo, L. Feng, J. Zhai, G. Wang, Y. Song, L. Jiang, D. Zhu, ChemPhysChem **5**, 750 (2004)
12. E. Martines, K. Seunarine, H. Morgan, N. Gadegaard, C.D.W. Wilkinson, M.O. Riehle, Nano Lett. **5**, 2097 (2005)
13. S. Boduroglu, M. Cetinkaya, W.J. Dressick, A. Singh, M.C. Demirel, Langmuir **23**, 11391 (2007)
14. S.M.M. Ramos, B. Canut, A. Benyagoub, J. Appl. Phys. **106**, 024305 (2009)
15. K. Robbie, J.C. Sit, M.J. Brett, J. Vac. Sci. Technol. B **16**, 1115 (1998)
16. Y.P. Zhao, D.X. Ye, G.C. Wang, T.M. Lu, Proc. SPIE **5219**, 59 (2003)
17. M.O. Jensen, M.J. Brett, Appl. Phys. A **80**, 763 (2005)
18. J.P. Singh, T. Karabacak, D.X. Ye, D.L. Liu, C. Picu, T.M. Lu, G.C. Wang, J. Vac. Sci. Technol. B **23**, 2114 (2005)
19. M. Suzuki, K. Nagai, S. Kinoshita, K. Nakajima, K. Kimura, T. Okano, K. Sasakawa, Appl. Phys. Lett. **89**, 133103 (2006)
20. D.P. Singh, J.P. Singh, J. Phys. Chem. C **115**, 11914 (2011)
21. D.P. Singh, P. Goel, J.P. Singh, J. Appl. Phys. **112**, 104324 (2012)
22. C.M. Zhou, D. Gall, Appl. Phys. Lett. **90**, 093103 (2007)
23. C. Petzig, C. Khare, B. Rauschenbach, Phys. Status Solidi B **6**, 1322 (2010)
24. J.G. Fan, X.J. Tang, Y.P. Zhao, Nanotechnology **15**, 501 (2004)
25. W.J. Khudhayer, R. Sharma, T. Karabacak, Nanotechnology **20**, 275302 (2009)
26. J.G. Fan, Y.P. Zhao, Langmuir **11**, 8245 (2010)
27. K.R. Khedir, G.K. Kannarpady, H. Ishihara, J. Woo, C. Ryerson, A.S. Biris, Langmuir **27**, 4661 (2011)
28. G.K. Kannarpady, K.R. Khedir, H. Ishihara, J. Woo, O.D. Oshin, S. Trigwell, C. Ryerson, A.S. Biris, Appl. Mater. Interfaces **3**, 2332 (2011)
29. M.O. Jensen, M.J. Brett, IEEE Trans. Nanotechnol. **4**, 269 (2005)
30. L. Abelmann, C. Lodder, Thin Solid Films **305**, 1 (1997)
31. H.V. Kranenburg, C. Lodder, Mater. Sci. Eng. R **11**, 295 (1994)
32. Y. Arima, T. Irisawa, J. Cryst. Growth **115**, 428 (1991)
33. K. Yoshida, K. Imagawa, Y. Honda, M. Futamoto, H. Daimon, Jpn. J. Appl. Phys. **27**, 1240 (1998)
34. A.B.D. Cassie, S. Baxter, Trans. Faraday Soc. **40**, 546 (1994)
35. J. Bico, C. Marzolin, D. Quere, Europhys. Lett. **47**, 220 (1999)
36. D. Quere, Physica A **313**, 32 (2002)
37. Z. Wang, N. Koratkar, Adv. Sci. Lett. **1**, 222 (2008)
38. R.N. Tait, T. Smy, M.J. Brett, Thin Solid Films **226**, 196 (1993)